

Vibrationally Excited C₄H

Andrew L. Cooksy,¹ C. A. Gottlieb,² T. C. Killian,³ P. Thaddeus,^{2,4} Nimesh A. Patel,² Ken H. Young,²
and M. C. McCarthy²

ABSTRACT

Rotational spectra in four new excited vibrational levels of the linear carbon chain radical C₄H radical were observed in the millimeter band between 69 and 364 GHz in a low pressure glow discharge, and two of these were observed in a supersonic molecular beam between 19 and 38 GHz. All have rotational constants within 0.4% of the X²Σ⁺ ground vibrational state of C₄H and were assigned to new bending vibrational levels, two each with ²Σ and ²Π vibrational symmetry. The new levels are tentatively assigned to the 1ν₆ and 1ν₅ bending vibrational modes (both with ²Π symmetry), and the 1ν₆ + 1ν₇ and 1ν₅ + 1ν₆ combination levels (²Σ symmetry) on the basis of the derived spectroscopic constants, relative intensities in our discharge source, and published laser spectroscopic and quantum calculations. Prior spectroscopic constants in the 1ν₇ and 2ν₇ levels were refined. Also presented are interferometric maps of the ground state and the 1ν₇ level obtained with the SMA near 257 GHz which show that C₄H is present near the central star in IRC+10216. We found no evidence with the SMA for the new vibrationally excited levels of C₄H at a peak flux density averaged over a 3'' synthesized beam of ≥ 0.15 Jy/beam in the 294 – 296 and 304 – 306 GHz range, but it is anticipated that rotational lines in the new levels might be observed in IRC+10216 when ALMA attains its full design capability.

1. Introduction

Carbon-rich asymptotic giant branch (AGB) stars are a principal source of carbonaceous gas and dust in the interstellar medium, and some of the material from which planets are ultimately formed (Molster & Waters 2003; Ott 2010). The dust is believed to form in the poorly explored inner envelope at $r \leq 5R_*$ where the temperatures and densities are high ($T = 800 - 2000$ K and $n_{\text{H}_2} = 10^9 - 10^{12}$ cm⁻³; Gail & Sedlmayr 1988; Cherchneff 2000; Agúndez & Cernicharo 2006). During the past 40 years, astronomers have studied the chemistry and dynamics in the outer envelope of the prototypical carbon-rich AGB star

IRC+10216, but it is only in the last few years that they have begun to observe a few small stable molecules in the inner envelope at high angular resolution with millimeter-wave interferometers.¹

In the first wide band interferometric spectral line survey of IRC+10216, a large population of narrow molecular emission lines were observed whose expansion velocities ($V_{\text{exp}} \sim 4$ km s⁻¹) are about three times lower than the terminal velocity (14.5 km s⁻¹; Patel et al. 2009a). Subsequent measurements at still higher angular resolution than the initial 3'' confirmed that the emission from the narrow lines arises in the dust formation zone close to the star (Patel et al. 2009b). In all, more than 200 narrow lines were observed in a 61 GHz wide spectral line survey in the 345 GHz band with the

¹Department of Chemistry and Biochemistry, San Diego State University, 5500 Campanile Drive, San Diego California 92182-1030

²Harvard-Smithsonian Center for Astrophysics, 60 Garden Street, Cambridge, MA 02138

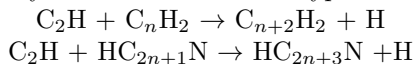
³Department of Physics and Astronomy and the Rice Quantum Institute, Rice University, Houston, Texas 77005-1892

⁴School of Engineering and Applied Sciences, Harvard University, Cambridge, Massachusetts 02138

¹Four small gaseous molecules have been identified in the dust formation zone from high resolution rotationally resolved spectra: CO (Patel et al. 2009b), HCN and HCCH (Fonfría et al. 2008), and HNC (Cernicharo et al. 2013). Lacking a permanent electric dipole moment, HCCH was only observed in the IR, and silicon carbide dust (SiC) is inferred from a broad featureless band in the IR at 11μm (Speck et al. 1997).

Submillimeter Array (SMA), of which the carriers of approximately 50% remain unassigned (Patel et al. 2011). When the same source was observed at somewhat higher angular resolution and sensitivity with ALMA, the number of unassigned lines is over 10 times greater (e.g., see the 1.9 GHz wide band near 267 GHz observed with a $0.6''$ diameter beam in ALMA Cycle 0 by Cernicharo et al. 2013). Detection of such a large number of unassigned lines confirms that the supporting laboratory spectroscopy is far from complete, and the chemistry in the inner envelope of carbon-rich AGB stars is not well understood.

After H_2 and CO , acetylene (HCCH) is the most abundant species in the inner envelope of IRC+10216 (Cherchneff 2000; Fonfría et al. 2008). Both on earth and in space, long carbon chain molecules are formed by reactions of highly reactive linear carbon chain C_nH radicals with closed shell acetylenic molecules of the type



(Millar et al. 2000; Woods et al. 2003). Rotational lines of seven C_nH radicals ($\text{C}_2\text{H} \cdots \text{C}_8\text{H}$) in the ground vibrational state have been studied extensively in the outer envelope of IRC+10216, and a few rotational lines have been observed in low-lying (bending) vibrational levels of C_2H , C_3H , C_4H , and C_6H at an angular resolution of $10'' - 30''$ with single antennas (see Table 1, and references therein). Chemical equilibrium calculations show that at temperatures near 1500 K, the abundance of the prototypical C_2H radical is comparable to that of HCCH (Yasuda & Kozasa 2012), but C_nH radicals have not yet been identified in the inner envelope.

In the course of measuring the rotational spectra of reactive acetylenic radicals, carbenes, and anions in a laboratory discharge through HCCH and a rare gas, we have observed rotational lines in four vibrationally excited levels of C_4H that had not previously been studied. Following the initial laboratory measurements of the C_4H radical in the ground vibrational state (Gottlieb et al. 1983), rotational lines were observed in IRC+10216 and a laboratory discharge which were tentatively assigned to the $2\nu_7$ ($^2\Sigma$) vibrational level (Guélin et al. 1987). At about the same time, Yamamoto et al. (1987) in a comprehensive laboratory study measured the rotational spectra in the ν_7 ($^2\Pi$) and

$2\nu_7$ ($^2\Delta$) excited vibrational levels, derived a full set of accurate spectroscopic constants for the $1\nu_7$ and $2\nu_7$ levels, obtained an approximate estimate of the ν_7 bending vibrational frequency, and assigned over 20 previously unidentified lines in the outer envelope of IRC+10216 to vibrationally excited C_4H in $1\nu_7$ and $2\nu_7$.

The spectroscopic constants derived from the rotational spectra and the symmetry of the new vibrational levels are well determined, but owing to the absence of either supporting quantum calculations or spectroscopic measurements in other wavelength bands, the assignments of the rotational spectra to particular vibrational levels were uncertain. However, with the recent laser spectroscopic measurements of previously unexplored bending vibrational levels in the ground $X^2\Sigma$ electronic state of C_4H (Mazzotti et al. 2011), we are now able to assign the rotational spectra to four vibrational levels. The assignments are based in part on the relative intensities of the rotational lines in our discharge source, and theoretical energies of the vibrational levels (Graf et al. 2001), whose accuracy was confirmed in part by the laser spectroscopic measurements (Mazzotti et al. 2011).

Here we present laboratory measurements of the rotational spectra in four new vibrational levels of C_4H in the millimeter band between 69 and 364 GHz (two each with $^2\Sigma$ and $^2\Pi$ vibronic symmetry), and the two $^2\Sigma$ levels in the centimeter band between 19 and 38 GHz. Also described are interferometric maps with the SMA of emission from the ground state and $1\nu_7$ level near 257 GHz, which show for the first time that C_4H is present near the central star. Further interferometric observations at higher angular resolution and sensitivity, might help establish whether other vibrationally excited C_nH radicals and small carbon bearing reactive species (such as the cumulene carbenes H_2C_n , etc.) are the carriers of some of the many unassigned lines that have been observed in the inner envelope of IRC+10216. Observations such as these might in turn help advance the chemistry of the inner envelope of carbon rich AGB stars in the region where dust begins to form.

2. Laboratory and Astronomical Measurements

2.1. Laboratory

The C_4H radical was observed at millimeter wavelengths with a free space gas discharge spectrometer used to study reactive radicals, carbenes, and molecular ions of astrophysical interest (Gottlieb et al. 2003). Rotational lines in vibrationally excited C_4H were measured under conditions which optimized the corresponding transitions in the ground vibrational state: a DC discharge (0.5 A, 1.4 kV) through a flowing mixture of helium (10–15%) and acetylene (HCCH) at a total pressure of 25 mTorr with the walls of the discharge cell cooled to 150 K. Although the most intense lines of C_4H were observed near 300 GHz, measurements with the free space spectrometer were extended to frequencies as low as 69 GHz in the three most intense new vibrational levels, and to 44 GHz in $1\nu_7$ ($^2\Pi$). Zeeman chopping with a 50 G magnetic field helped discriminate between paramagnetic species and interfering closed shell species present in the discharge.

The frequencies of the rotational lines were derived from a simultaneous least-squares fit of the explicit expression for the second derivative of a theoretical Lorentzian profile, and an n^{th} order polynomial to spectra observed at 512 points in a 10 MHz bandwidth (see Gottlieb et al. 2003). The S/N in the raw unsmoothed spectra were about 10 in approximately 15 min of integration (Figure 1). Because the line widths were typically about 800 kHz (FWHM), the second derivative line profile was sampled at approximately 70 points between the two horns (or satellites). From prior work on similar systems, we estimate that the uncertainties in the measured frequencies are about 20 kHz, or less than 0.1 km s^{-1} for lines up to 363 GHz.

Three rotational transitions were also observed in the centimeter band with our Fourier transform microwave (FTM) spectrometer (McCarthy et al. 2000) in $2\nu_2$ and the two new ones with $^2\Sigma$ symmetry (see sample spectra in Figure 2). The discharge conditions were optimized on the corresponding rotational transition of C_4H in the ground vibrational state: a 1050 V DC discharge in the throat of the supersonic nozzle of the spectrometer through a mixture of acetylene (0.1%)

heavily diluted in neon. Typical gas flow rates were $25 \text{ cm}^{-3} \text{ min}^{-1}$ at standard temperature and pressure (STP), a pulse repetition rate of 6 Hz, pulse duration of 300 μs , and stagnation pressure behind the nozzle of 2.5 kTorr. Under these conditions, lines in the $1\nu_7$ and $2\nu_7$ levels were 100–400 times less intense than those of the ground state.

2.2. Astronomical

Spectra and maps of C_4H in IRC+10216 were observed with seven antennas of the SMA in the compact configuration on 6 March 2008, at baselines between 16.4 and 77.0 m. The synthesized beam was $2.92'' \times 2.60''$ at a position angle (P.A.) of 72° , and the field of view (size of primary beam) was $\sim 46''$. The system temperature ranged from 200 to 350 K, $\tau_{225 \text{ GHz}} \sim 0.20$, and the total on source integration time was about 10 hours. The correlator was configured for a uniform frequency resolution of 0.64 MHz per channel in the lower and upper 2 GHz wide sidebands with band centers at 256.4 and 266.4 GHz. The quasar 0854+201 was observed every 20 min for gain calibration. The spectral bandpass was calibrated by observations of 3C273 and Jupiter, and absolute flux calibration by observations of Mars and Titan.

3. Results

3.1. Laboratory Spectroscopic

Four new series of satellite lines were assigned to rotational transitions in vibrationally excited C_4H because: (1) the rotational and centrifugal distortion constants (B and D) are within 0.4% of those in the ground state (see Figure 3); and (2) the analogous satellite lines were observed in C_4D , when HCCH was replaced by DCCD in our discharge. The symmetries of the four new vibrational levels were established from the following considerations. Two quartets, symmetrically displaced about a central frequency, were assigned to two new $^2\Pi$ levels (designated $a^2\Pi$ and $b^2\Pi$). The quartets, consisting of four lines with comparable intensities in each rotational transition, precluded levels with $^2\Sigma$ symmetry and the well-resolved K -doubling implied that $K = 1$. The remaining two series were assigned to $^2\Sigma$ levels ($a^2\Sigma$ and $b^2\Sigma$), because only two lines were found in each series and the coupling case remained Hund's case (b)

at all observed frequencies. Although doublets (rather than quartets) are frequently observed in levels with $K > 1$ because the K -doubling is often unresolved (e.g., in ${}^2\Delta$ levels), there is a significant departure from case (b) coupling in the lower rotational transitions in vibrational levels with $K > 1$ owing to the spin-orbit interaction. Listed in Tables 2–8 are the measured rotational lines in the four new vibrational levels, and some new measurements in the previously studied $1\nu_7$ (${}^2\Pi$) and $2\nu_7$ (${}^2\Sigma$ and ${}^2\Delta$) levels.

In a closed shell molecule, l -type doubling is described by only one constant (q), but two constants (p and q) are needed to describe K -type doubling in molecules with vibrational and electronic contributions (Brown 1975). In the well studied C_2H radical, the $A^2\Pi$ excited electronic state is 3600 cm^{-1} above the $X^2\Sigma$ ground state and p is much smaller than q , implying that the vibrational contribution to the K -type doubling is dominant (Killian et al. 2007; Sharp-Williams et al. 2011). However, p and q are comparable in C_4H , because the $A^2\Pi$ state is much closer to ground (222 cm^{-1} ; Mazzotti et al. 2011), and the vibronic interaction between the two electronic states in C_4H is much greater than in C_2H .

The rotational spectra in the vibrationally excited levels of C_4H were analyzed by essentially the same method as previously applied to vibrationally excited C_2H (Killian et al. 2007, and references therein). In this approach, the rotational structure in each vibrational level was described by an effective Hamiltonian used to analyze an isolated electronic state in a diatomic molecule. In open shell molecules, the electron orbital (Λ) and vibrational (l) angular momentum are coupled, and Λ -type and l -type doubling combine to produce K -type doubling. It has been shown in work similar to that here that the rotational spectra in excited vibrational levels of open shell molecules are reproduced to very high accuracy by this approach. Some rotational levels in $b^2\Sigma$ and $b^2\Pi$ were perturbed by nearby vibrational levels, requiring two additional terms in the Hamiltonian to reproduce the spectrum of $b^2\Sigma$ (see Section 3.1.1).

We have adhered to the sign convention in Killian et al. (2007), in which the sign of K -doubling constant q was determined on the assumption that the hyperfine doubling constant d is positive. Following this convention, q is negative in $1\nu_7$ (${}^2\Pi$).

Although d is not well determined in the $b^2\Pi$ level, q is assumed to be negative in $b^2\Pi$ as well. Because the hyperfine constants were not determined in the $a^2\Pi$ level, we assumed by analogy with $1\nu_7$ (${}^2\Pi$) and $b^2\Pi$ that p is also negative in the $a^2\Pi$ level. The signs of γ and the hyperfine coupling constants b_F and c are the same as those in the ground state as expected, because the spin-rotation and hyperfine interactions are sufficiently decoupled from vibrational effects. The spin-orbit constant A is negative in the $1\nu_7$ (${}^2\Pi$), $2\nu_7$ (${}^2\Delta$), $a^2\Pi$, and $b^2\Pi$ vibrational levels of the $X^2\Sigma$ ground electronic state, because A is negative in the low-lying $A^2\Pi$ excited electronic state (Mazzotti et al. 2011).

3.1.1. Perturbations

The $b^2\Sigma$ and $b^2\Pi$ levels exhibit pronounced N -dependent perturbations by vibrational levels that were not observed in this study. In $b^2\Sigma$, the interacting levels cross between $N = 15$ and 25 , resulting in very large shifts in the transition frequencies of one of the spin-rotation components, whereas the other component is not perturbed. To fit this pattern, a standard Coriolis-type contribution,

$$\Delta E = \frac{q_l(N^2 - 1)}{1 + \rho N(N + 1)}, \quad (1)$$

was added to the energies of the perturbed component. The N -dependence of the numerator depends on the specific spin-rotation components in the interaction. We chose the pair that gave the lowest standard deviation of the fit, but q_l differs by $\leq 10\%$ for other choices and the constants differ by less than one standard deviation. In $b^2\Pi$, all four components are weakly perturbed and the magnitude of the perturbation increases with increasing N . Analyzing the perturbation in $b^2\Pi$ would require adding several empirical parameters with no clear interpretation. Instead, the two most strongly perturbed transitions in $b^2\Pi$ were removed from the fit, and $b^2\Pi$ was treated as though it were an isolated ${}^2\Pi$ state (see Table 6).

$b^2\Sigma$

The strong perturbation of the $N = J + \frac{1}{2}$ component of the spin-rotation doublets in $b^2\Sigma$ implies that there is an interaction with a level with either ${}^2\Pi$ or ${}^2\Sigma^-$ vibronic symmetry. To first order in

perturbation theory, $q_l = \beta^2/\Delta\nu$ and $\rho = \Delta B/\Delta\nu$ in Eq. (1), where $\Delta\nu$ is the difference in band origins $\nu_0(b^2\Sigma) - \nu_0(x)$, $\Delta B = B(b^2\Sigma) - B(x)$, the perturbing level is labeled x , and β is the coefficient of the Coriolis coupling matrix element. Both q_l and ρ in $b^2\Sigma$ are negative (Table 10), indicating that the perturbing level has a smaller B and the band origin is higher than $b^2\Sigma$.

$b^2\Pi$

The $b^2\Pi$ level is perturbed at high N by a level that has not yet been identified. When the two uppermost rotational lines from any one of the four parity/spin-orbit branches are removed from the fit, the rms is reduced by a factor of two and the higher order distortion terms L and p_H are not needed. In Table 10, transitions with $N' > 20$ in $J = N - \frac{1}{2} e$ were omitted because doing so yielded the lowest rms, but other fits with comparable rms were obtained if one of the other branches was neglected instead. The addition of higher-order terms in the Hamiltonian such as q_H , implies that more than one branch is significantly perturbed. A perturbation analysis similar to that for $b^2\Sigma$ was not attempted for $b^2\Pi$, primarily because the frequency shifts are much smaller in $b^2\Pi$. In the future, measurements of the perturbing levels near the resonance interactions in $b^2\Sigma$ and $b^2\Pi$ might yield accurate coupling constants and frequency separations of the perturbing levels.

3.1.2. Assignment of Vibrational Modes

The vibrational modes of C_4H may be loosely divided into C–H local modes (ν_1 stretch and ν_5 bend), and C_4 normal modes (ν_2 and ν_4 symmetric stretches, ν_3 antisymmetric stretch, and ν_6 and ν_7 bends). For the most likely ones observed here ($\nu_4, \nu_5, \nu_6, \nu_7$, and combinations thereof), accurate estimates of the band origins of three (ν_4, ν_7 , and $\nu_6 + \nu_7$) were recently derived from laser spectroscopic double resonance four-wave mixing measurements of the $B^2\Pi - X^2\Sigma^+$ electronic band near 24,000 cm^{-1} (Mazzotti et al. 2011). Theoretical frequencies of all seven vibrational modes were calculated independently in the harmonic approximation (Graf et al. 2001). Because the theoretical frequencies of ν_4 and ν_7 agree to within 6% or better with those measured by Mazzotti et al., the theoretical frequencies of ν_5 and ν_6 are likely

known to comparable accuracy (see Table 11).

Owing to the precision of the frequency measurements and degree of symmetry in the rotational spectra here, the vibronic symmetries and spectroscopic constants of the four new levels in C_4H were determined to a very high level of confidence. Because the rotational information needed to guide the assignment of the new vibrational levels of C_4H was not available either from theoretical calculations or IR spectroscopic measurements, the assignments to particular vibrational levels is tentative.

Rotational spectra in vibrational satellites of closed shell polyatomic molecules are routinely assigned on the basis of relative intensities of the lines, vibronic symmetry, the magnitude and sign of the vibration-rotation interaction α (where $B_v - B_0 = -v\alpha$), and the l -doubling constant q , where the approximations

$$\alpha(v_1, v_2, v_3, \dots) = v_1\alpha_1 + v_2\alpha_2 + v_3\alpha_3 + \dots \quad (2)$$

and

$$q_n = 2.6 \frac{B^2}{\nu_n} \quad (3)$$

are normally accurate to within 20% for low vibrational excitation. For example, in the well studied linear cyanopolyynes HCN and HCCCN (Mbosei et al. 2000), the magnitude of α increases as the fundamental frequency of the mode decreases, it is negative in bending levels ($B_v^{\text{bend}} > B_0$), and positive in stretching levels ($B_v^{\text{stretch}} < B_0$) as expected. Unfortunately, the standard procedure for assigning rotational spectra to specific vibrational levels in closed shell polyatomic molecules is not necessarily applicable in the open shell C_nH radicals. For example, α in the $1\nu_7$ level of C_4H is $1/5$ that in $2\nu_7$, rather than $1/2$ as expected from Eq. 2. Similarly, the α 's in the bending vibrational levels in C_2H are anomalous: α in the $1\nu_2$ level is $1/12$ that in $2\nu_2$, rather than $1/2$ as expected (Killian et al. 2007).

Assignments of the new vibrationally excited levels of C_4H were restricted to levels with $^2\Sigma$ and $^2\Pi$ symmetry, and to ones whose magnitude of α are among the smallest. Before considering higher excitations with $v \geq 2$ and higher-lying combination levels, we examined the fundamental modes (ν_4, ν_5, ν_6 , and ν_7) and combinations with the ν_7 bend. The requirement that the rotational frequencies in the new vibrational levels

are close to those of the ground state, implies that they are Hund’s case (*b*) coupled in the frequency range where most of the measurements were made (i.e., at $N \approx 30$). Because the spin-orbit interaction is small, the vibration-rotation coupling increases with increasing vibrational excitation (as indicated by Eq. 2, and observed in HCCCN; Mbosei et al. 2000), implying that rotational lines in the lower vibrational levels lie in the frequency band that we had covered.

3.1.3. Spectroscopic considerations

There are many vibrational levels in the ground $X^2\Sigma$ and excited $A^2\Pi$ electronic states of C_4H below 1000 cm^{-1} (see Figure 6 in Mazzotti et al. 2011). Considering only those in the $X^2\Sigma$ electronic state, (excluding $1\nu_7$ and $2\nu_7$) there are eight possible candidates.² Three of these, all with excitation energies between 400 and 600 cm^{-1} , were considered as candidates for the two new vibrational levels with Π symmetry: $1\nu_6$, $1\nu_5$, and $3\nu_7$. We have assumed on the basis of the qualitative form of Eq. 2, that α in $3\nu_7$ is significantly larger than in $2\nu_7$. Therefore the $3\nu_7$ level was ruled out, because the rotational lines in the levels we observe are closer in frequency to the ground state lines than those in $2\nu_7$. As a result, the $b^2\Pi$ level was assigned to $1\nu_6$, and the less intense $a^2\Pi$ level to the higher lying $1\nu_5$ level.

There are seven candidates (between 600 and 1000 cm^{-1} above ground) for the two new levels with Σ symmetry. The $4\nu_7$ level was discounted, owing to the large α and intensity considerations (see Section 3.1.4). The $a^2\Sigma$ level was assigned to the $\nu_6 + \nu_7$ combination level, even though the magnitude of α is very small for a combination level and the $^2\Delta$ and the second $^2\Sigma$ level were not observed, because $\nu_6 + \nu_7$ has the lowest energy of the remaining levels with Σ symmetry. The $b^2\Sigma$ level was assigned last, because it was made primarily on the basis of the intensity information discussed in Section 3.1.4.

3.1.4. Intensity considerations

Assignments of the vibrational levels of C_4H on the basis of relative intensities might be se-

cure if the vibrational temperature (T_{vib}) in our HCCH discharge were known precisely. Our best independent estimate of T_{vib} is from prior work on the C_2H radical because: (1) the electronic and vibrational level structures of C_2H and C_4H are qualitatively similar; (2) both radicals are observed under comparable excitation conditions in the same HCCH discharge; and (3) there is a large body of IR measurements and extensive quantum calculations of the vibrational level structure in C_2H (Sharp-Williams et al. 2011, and references therein). We found that T_{vib} in the bending vibration (010), and the combination levels (110) and (011) of C_2H is $100 - 200\text{ K}$ higher than the temperature of the wall of our discharge cell (150 K), whereas T_{vib} in the stretching levels (100) and (001) is about 5 times higher ($\sim 1500\text{ K}$; Killian et al. 2007). By analogy with C_2H , it was anticipated that $T_{\text{vib}} = 250 - 350\text{ K}$ would also apply to C_4H in ν_5, ν_6, ν_7 , and in levels in combination with the bending vibrations. As a test, we first examined the excitation of $1\nu_7$ and $2\nu_7$ in C_4H , because the assignments and the vibrational energies are well established (Yamamoto et al. 1987; Mazzotti et al. 2011). The derived vibrational temperature for the $1\nu_7$ and $2\nu_7$ levels in C_4H ($T_{\text{vib}} = 311 \pm 66\text{ K}$) is in good agreement with that of C_2H ($370 \pm 120\text{ K}$) and C_2D ($260 \pm 60\text{ K}$; Killian et al. 2007), therefore the analogy with C_2H appears justified.

Encouraged by the similarity between the vibrational excitation of C_2H and the lowest bending vibrational levels of C_4H , we then considered the intensity information when assessing the assignments of the new levels that have been made on the basis of the spectroscopic constants (Section 3.1.3). The $1\nu_4$ level at 930 cm^{-1} (1337 K ; Mazzotti et al. 2011) was ruled out because $T_{\text{vib}} \sim 450\text{ K}$ is much too low for a stretching vibration, and the intensity is much too high if $b^2\Sigma$ were a combination level with a bending vibration (e.g., $\nu_4 + \nu_7$ at 1579 K above ground). On the assumption that T_{vib} is comparable to that of the $1\nu_7$ and $2\nu_7$ bending vibrational levels, the most plausible assignment of $b^2\Sigma$ is the combination level $\nu_5 + \nu_7$. The vibrational energy of $b^2\Sigma$ derived from Figure 4 ($1015 \pm 98\text{ K}$, or $706 \pm 68\text{ cm}^{-1}$) is in good agreement with the theoretical frequency (756 cm^{-1} ; Graf et al. 2001). With these assignments, the relative intensities of all six vibrational levels of C_4H observed in our discharge are charac-

²The eight candidates in the $X^2\Sigma$ electronic state are $(\nu_4, \nu_5, \nu_6, \nu_7) = (0003), (0004), (0010), (0100), (1000), (0011), (0101),$ and (1001) .

terized by a vibrational temperature (338 ± 31 K; Figure 4) that is consistent with the bending vibrational levels of C_2H .

3.2. Astronomical Observations

Shown in Figure 5, are channel maps of the $N = 27 \rightarrow 26$ rotational transition of C_4H near 257 GHz in the ground vibrational state, and the $1\nu_7$ (${}^2\Pi$) excited vibrational level. The rotational transitions observed here are about 2.5 times higher in frequency, and 150 K higher in energy (E_u) than those observed earlier in the 3 mm band with the IRAM Plateau de Bure Interferometer (PdBI) by Guélin et al. (1999). The peak flux density is 0.63 Jy/beam for the average of both spin components in the ground state, and 0.34 Jy/beam for three of the four rotational transitions in the vibrationally excited level. Also shown are integrated intensity maps of the same transitions in the ground state and excited vibrational level, for a velocity interval corresponding to the middle two rows in the channel maps (from -33 and -18 km s^{-1} in Figure 5) that is roughly centered on the systemic velocity of -26 km s^{-1} (see Figures 6 and 7).

As noted earlier by Guélin et al. (1999), the ground and excited emission of C_4H follow each other very closely in the outer envelope. Here for the first time, both ground and vibrationally excited C_4H are observed near the central star. The exact nature of the emission near the central star remains unclear from our SMA observations — i.e., whether it is from a smaller expanding inner shell that has not reached the terminal velocity (~ 15 km s^{-1}), or an asymmetrical structure connecting the outer shell to the inner envelope. Interpretation of the central emission will require further interferometric observations at higher S/N and with a much better u - v coverage. The clumpy features in the expanding shell structure illustrates the inherent uncertainties when comparing the interferometric measurements with published chemical models (which typically show only radial dependence). As expected, the flux density in the ground and vibrationally excited emission in the central region (0.6 versus 0.4 Jy/beam) is comparable at the higher kinetic temperature of the gas (Fonfría et al. 2008).

We also examined the 345 GHz spectral line survey with the SMA (Patel et al. 2011) for possi-

ble evidence of the four new excited bending vibrational levels of C_4H , but none was found at peak flux densities averaged over a $3''$ synthesized beam of ≥ 0.15 Jy in the 294 – 296 and 304 – 306 GHz range.

4. Discussion

It has generally been assumed that C_4H (and other C_nH radicals) is confined to the outer envelope of IRC+10216, because that is what is implied from the spectral line profiles of the ground and $1\nu_7$, $2\nu_7$ (${}^2\Sigma$), and $2\nu_7$ (${}^2\Delta$) excited vibrational levels observed at low angular resolution with single antennas. Furthermore, interferometric maps of rotational transitions of C_4H in the ground vibrational and the lowest excited vibrational level $1\nu_7$ in the 3 mm band, show that the emission is confined to a thin ($3''$ thick) shell in the outer envelope with a radius (r) of $15''$ (Guélin et al. 1999) — just as most chemical models predict. However, Cordiner & Millar (2009) recently showed that when density-enhanced dust shells are included in the chemical models, C_4H is predicted to be present in a thick inner ring ($r \sim 8''$) in addition to the outer ring at $15''$.

Rotational lines in the four new vibrational levels of C_4H will most likely be observed in the inner envelope of IRC+10216, because that is where these higher lying levels will be most populated owing to the higher densities and temperatures closer to the star. Although we did not find any evidence for lines of the new excited bending vibrational levels of C_4H , it is plausible that the new vibrationally excited levels of C_4H will be observed when millimeter-wave interferometers attain higher sensitivity now that we have established that C_4H is present near the central star.

Direct observations of HCCH in the IR and HNC in the millimeter band, provide a template for assigning and analyzing rotational spectra in vibrationally excited levels of C_nH radicals among the many unassigned features recently observed in the inner envelope of IRC+10216 with interferometers. These include: (1) a detailed analysis of the kinetic, vibrational, and rotational temperatures of HCCH at $1R_\star \leq r \leq 300R_\star$ derived from rotationally resolved vibrational lines in the 11 – 14 μm band (Fonfría et al. 2008); (2) observations of HNC in the dust formation zone near

270 GHz with ALMA Cycle 0, and an accompanying detailed radiative transfer analysis (Cernicharo et al. 2013); and (3) a related observation of HCCCN in the dense core of the protoplanetary nebula CRL 618 with the SMA in the 345 GHz band at $r < 0.7''$ from the central star where $T = 400 - 600$ K (Lee et al. 2013).

Sample spectra obtained in ALMA Cycle 0 with sixteen 16 m diam antennas and a $0.6''$ synthesized beam in the 263 – 272 GHz band (Cernicharo et al. 2013) are about 7 times more sensitive than those in the SMA survey in the 345 GHz band (Patel et al. 2011).³ Referring to Figure 1 in Cernicharo et al. (2013), the peak flux densities of most of the unassigned narrow lines observed with ALMA (≤ 0.15 Jy/beam) are below the detection limit with the SMA. When ALMA attains full design sensitivity with 66 antennas it will be about 4 times more sensitive still, offering great promise for the identification of key reactive molecular intermediates such as the C_nH radicals in the inner envelope of the prototypical carbon rich AGB star IRC+10216, and elucidation of the chemical processes crucial to the formation of carbonaceous dust in the interstellar gas.

REFERENCES

- Agúndez, M., & Cernicharo, J. 2006, ApJ, 650, 374
- Brown, J. M. 1975, J. Mol. Spectrosc., 56, 159
- Caris, M., Giesen, T. F., Duan, C., Müller, H. S. P., Schlemmer, S., & Yamamda, K. M. T. 2009, J. Mol. Spectrosc., 253, 99
- Cernicharo, J., Guélin, M., Agúndez, M., McCarthy, M. C., & Thaddeus, P. 2008, ApJ, 688, L83
- Cernicharo, J., Daniel, F., Castro-Carrizo, A., Agúndez, M., Marcelino, N., Joblin, C., Goicoechea, J. R., & Guélin, M. 2013, ApJ, 778, L25
- Cherchneff, I. 2000, A&A, 456, 1001
- Cordiner, M. A., & Millar, T. J. 2009, ApJ, 697, 68
- Fonfría, J. P., Cernicharo, J., Richter, M. J., & Lacy, J. H. 2008, ApJ, 673, 445
- Gail, H.-P., & Sedlmayr, E. 1988, A&A, 206, 153
- Gottlieb, C. A., Gottlieb, E. W., Thaddeus, P., & Kawamura, H. 1983, ApJ, 275, 916
- Gottlieb, C. A., McCarthy, M. C., & Thaddeus, P. 2010, ApJS, 189, 261
- Gottlieb, C. A., Myers, P. C., & Thaddeus, P. 2003, ApJ, 588, 665
- Graf, S., Geiss, J., & Leutwyler, S. 2001, J. Chem. Phys., 114, 4542
- Guélin, M., Cernicharo, J., Navarro, S., Woodward, D. R., Gottlieb, C. A., & Thaddeus, P. 1987, A&A, 182, L37
- Guélin, M., Neininger, N., Lucas, R., & Cernicharo, J. 1999, in Proc. 3rd Cologne-Zermatt Symp., The Physics and Chemistry of the Interstellar Medium, ed. V. Ossenkopf (Herdecke: CGA-Verlag), 326
- Killian, T. C., Gottlieb, C. A., & Thaddeus, P. 2007, J. Chem. Phys., 127, 114320
- Lee, C.-F., Yang, C.-H., Sahai, R., & Sánchez Contreras, C. 2013, ApJ, 770, 153
- Mazzotti, F. J., Raghunandan, R., Esmail, A. M., Tulej, M., & Maier, J. P. 2011, J. Chem. Phys., 134, 164303
- Mbosei, L., Fayt, A., Dréan, P., & Cosléou, J. 2000, J. Mol. Struct., 517-518, 271
- McCarthy, M. C., Chen, W., Travers, M. J., & Thaddeus, P. 2000, ApJS, 129, 611
- Millar, T. J., Herbst, E., & Bettens, R. P. A. 2000, MNRAS, 316, 195
- Molster, F. J., & Waters, L. B. F. M. 2003, in *Astromineralogy*, ed. by T. Henning (Springer, New York, 2003), pp. 121-170
- Ott, U. 2010, in *Astromineralogy*, by T. Henning. Lecture notes in Physics, Vol. 815 (Springer, Berlin, 2010), pp. 277-311

³The collecting area of ALMA Cycle 0 was 14 times greater, but the integration time (with overhead) was about 3 – 4 times greater with the SMA. The synthesized beam in ALMA Cycle 0 was 5 times smaller, but the diameter of the inner envelope ($0.2''$) is small with respect to the angular resolution in both observations.

- Patel, N. A, Young, K. H., Brünken, S., et al. 2009a, ApJ, 692, 1205
- Patel, N. A, Young, K. H., Brünken, S., Menten, K. M., Thaddeus, P., & Wilson, R. W. 2009b, ApJ, 691, L55
- Patel, N. A, Young, K. H., Gottlieb, C. A., et al. 2011, ApJS, 193, 17
- Sharp-Williams, E. N., Roberts, M. A., & Nesbitt, D. J. 2011, J. Chem. Phys., 134, 064314
- Speck, A., Barlow, M. J., & Skinner, C. J. 1997, MNRAS, 288, 431
- Tenenbaum, E. D., Dodd, J. L., Milam, S. N., Wolf, N. J., & Ziurys, L. M. 2010, ApJS, 190, 348
- Woods, P. M., Millar, T. J., Herbst, E., & Zijlstra, A. A. 2003, A&A, 402, 189
- Yamamoto, S., Saito, S., Guélin, M., Cernicharo, J., Suzuki, H., & Ohishi, M. 1987, ApJ, 323, L149
- Yamamoto, S., Saito, S., Suzuki, H., Deguchi, S., Kaifu, N., Ishikawa, S.-I., & Ohishi, M. 1990, ApJ, 348, 363
- Yasuda, Y., & Kozasa, T. 2012, ApJ, 745, 159

TABLE 1
VIBRATIONALLY EXCITED C_nH RADICALS IN IRC+10216

Molecule	Level ^a	Band Origin ^b (cm ⁻¹)	Beamwidth ($''$)	Flux ^c (Jy)	Reference	
					Space	Lab
C ₂ H	1ν ₂ (² Π)	370	29	0.3	d	e
C ₃ H	1ν ₄ (² Σ ^u)	27	28	0.4	d	f
C ₄ H	1ν ₇ (² Π)	170	27	2.9	d	g
	2ν ₇ (² Σ)	375	27	1.5	d	g
	2ν ₇ (² Δ)	375	27	0.6	d	g
C ₆ H	ν ₁₁ ? (² Σ)	14	28	0.1	h	i
	ν ₁₁ ? (² Δ)	73	28	0.04	h	i

^aVibrational levels whose rotational spectra have been observed in IRC+10216.

^bApproximate energy of the band origin above ground.

^cPeak flux density of the fine and hyperfine structure resolved rotational transition averaged over the single antenna beam.

^dTenenbaum et al. (2010)

^eKillian et al. (2007)

^fCaris et al. (2009), and references therein.

^gYamamoto et al. (1987)

^hCernicharo et al. (2008)

ⁱGottlieb et al. (2010)

TABLE 2
MEASURED ROTATIONAL FREQUENCIES IN THE $1\nu_7$ (${}^2\Pi$) EXCITED VIBRATIONAL LEVEL OF C_4H

$N' \leftarrow N$	$J = N - \frac{1}{2}$				$J = N + \frac{1}{2}$			
	Parity	$F' \leftarrow F$	Frequency (MHz)	$O - C^a$ (MHz)	Parity	$F' \leftarrow F$	Frequency (MHz)	$O - C^a$ (MHz)
5 \leftarrow 4	<i>f</i>	4 \leftarrow 3	44712.367	0.036				
	<i>f</i>	5 \leftarrow 4	44712.913	0.007				
	<i>e</i>	4 \leftarrow 3	44830.238	-0.018				
	<i>e</i>	5 \leftarrow 4	44830.966	0.010				
7 \leftarrow 6					<i>e</i>	8 \leftarrow 7	68553.686	0.025
					<i>e</i>	7 \leftarrow 6	68554.209	0.022
					<i>f</i>	8 \leftarrow 7	68716.586	-0.008
					<i>f</i>	7 \leftarrow 6	68717.020	0.004
8 \leftarrow 7	<i>f</i>	7 \leftarrow 6	74141.426	0.001	<i>e</i>	9 \leftarrow 8	77833.064	-0.005
	<i>f</i>	8 \leftarrow 7	74141.841	0.003	<i>e</i>	8 \leftarrow 7	77833.510	-0.024
	<i>e</i>	7 \leftarrow 6	74352.312	0.015	<i>f</i>	9 \leftarrow 8	78029.136	0.020
	<i>e</i>	8 \leftarrow 7	74352.817	-0.002	<i>f</i>	8 \leftarrow 7	78029.504	0.024
9 \leftarrow 8	<i>f</i>	8 \leftarrow 7	83878.977	-0.019	<i>e</i>	10 \leftarrow 9	87142.553	0.005
	<i>f</i>	9 \leftarrow 8	83879.350	-0.003	<i>e</i>	9 \leftarrow 8	87142.954	-0.002
	<i>e</i>	8 \leftarrow 7	84122.980	0.021	<i>f</i>	10 \leftarrow 9	87371.839	-0.027
	<i>e</i>	9 \leftarrow 8	84123.434	0.013	<i>f</i>	9 \leftarrow 8	87372.159	-0.019
10 \leftarrow 9	<i>f</i>	9 \leftarrow 8	93585.949	-0.022				
	<i>f</i>	10 \leftarrow 9	93586.275	-0.003				
	<i>e</i>	9 \leftarrow 8	93863.168	-0.011				
	<i>e</i>	10 \leftarrow 9	93863.572	-0.013				

^aFrequencies calculated with the constants in Table 9.

TABLE 3
MEASURED ROTATIONAL FREQUENCIES IN THE $2\nu_7$ (${}^2\Sigma$) EXCITED VIBRATIONAL LEVEL OF C_4H

$N' \leftarrow N$	$J = N - \frac{1}{2}$			$J = N + \frac{1}{2}$		
	$F' \leftarrow F$	Frequency (MHz)	$O - C^a$ (MHz)	$F' \leftarrow F$	Frequency (MHz)	$O - C^a$ (MHz)
2 \leftarrow 1	2 \leftarrow 1	19157.642	0.002	3 \leftarrow 2	19100.146	0.000
3 \leftarrow 2	3 \leftarrow 2	28721.504	-0.003	3 \leftarrow 2	28664.320	-0.002
	2 \leftarrow 1	28721.625	-0.001	4 \leftarrow 3	28664.476	0.002
4 \leftarrow 3	4 \leftarrow 3	38285.562	0.000	4 \leftarrow 3	38228.637	-0.002
	3 \leftarrow 2	38285.583	0.002	5 \leftarrow 4	38228.734	0.002

NOTE.—Estimated 1σ uncertainties in the centimeter-wave measurements is 5 kHz.

^aFrequencies calculated with the constants in Table 9.

TABLE 4
MEASURED ROTATIONAL FREQUENCIES IN THE $2\nu_7$ (${}^2\Delta$) EXCITED VIBRATIONAL LEVEL OF C_4H

$N' \leftarrow N$	$J = N - \frac{1}{2}$			$J = N + \frac{1}{2}$		
	$F' \leftarrow F$	Frequency (MHz)	$O - C^a$ (MHz)	$F' \leftarrow F$	Frequency (MHz)	$O - C^a$ (MHz)
7 \leftarrow 6				8 \leftarrow 7	69192.595	0.020
				7 \leftarrow 6	69193.060	0.007
8 \leftarrow 7	7 \leftarrow 6	74161.246	0.017	9 \leftarrow 8	78519.431	0.009
	8 \leftarrow 7	74161.662	0.019	8 \leftarrow 7	78519.898	0.033
9 \leftarrow 8	8 \leftarrow 7	83947.326	-0.002	10 \leftarrow 9	87870.583	-0.013
	9 \leftarrow 8	83947.724	0.003	9 \leftarrow 8	87870.967	-0.033
10 \leftarrow 9	9 \leftarrow 8	93708.740	0.001			
	10 \leftarrow 9	93709.107	0.003			

^aFrequencies calculated with the constants in Table 9.

TABLE 5
MEASURED ROTATIONAL FREQUENCIES IN THE $a^2\Pi$ EXCITED VIBRATIONAL LEVEL OF C_4H

$N' \leftarrow N$	$J = N - \frac{1}{2}$			$J = N + \frac{1}{2}$		
	Parity	Frequency (MHz)	$O - C^a$ (MHz)	Parity	Frequency (MHz)	$O - C^a$ (MHz)
10 \leftarrow 9	<i>e</i>	95502.793	0.032	<i>f</i>	95557.501	0.028
	<i>f</i>	95542.080	0.031	<i>e</i>	95609.099	0.014
13 \leftarrow 12	<i>e</i>	124182.153	-0.006	<i>f</i>	124198.118	0.012
	<i>f</i>	124235.243	-0.024	<i>e</i>	124263.526	-0.008
15 \leftarrow 14	<i>e</i>	143293.623	-0.030	<i>f</i>	143295.568	-0.009
	<i>f</i>	143356.034	-0.004	<i>e</i>	143370.299	0.019
18 \leftarrow 17	<i>e</i>	171954.051	0.000	<i>f</i>	171942.999	-0.028
	<i>f</i>	172030.463	-0.008	<i>e</i>	172031.797	0.032
19 \leftarrow 18	<i>e</i>	181506.072	-0.037			
	<i>f</i>	181587.188	-0.056	<i>e</i>	181585.504	-0.016
30 \leftarrow 29	<i>e</i>	286540.183	0.012	<i>f</i>	286510.241	-0.079
	<i>f</i>	286674.782	0.010	<i>e</i>	286657.242	0.004
38 \leftarrow 37	<i>e</i>	362881.183	0.024	<i>f</i>	362847.399	0.015
	<i>f</i>	363057.084	0.053	<i>e</i>	363035.520	-0.053

^aFrequencies calculated with the constants in Table 10.

TABLE 6
MEASURED ROTATIONAL FREQUENCIES IN THE $b^2\Pi$ EXCITED VIBRATIONAL LEVEL OF C_4H

$N' \leftarrow N$	$J = N - \frac{1}{2}$				$J = N + \frac{1}{2}$			
	Parity	$F' \leftarrow F$	Frequency (MHz)	$O - C^a$ (MHz)	Parity	$F' \leftarrow F$	Frequency (MHz)	$O - C^a$ (MHz)
7 ← 6					<i>f</i>	8 ← 7	69557.920	0.032
					<i>f</i>	7 ← 6	69558.338	-0.018
					<i>e</i>	8 ← 7	69689.931	0.026
					<i>e</i>	7 ← 6	69690.356	0.029
8 ← 7	<i>e</i>	7 ← 6	73404.509	0.034				
	<i>e</i>	8 ← 7	73404.924	0.021				
	<i>f</i>	7 ← 6	73600.331	0.008	<i>e</i>	9 ← 8	79038.104	-0.017
9 ← 8	<i>f</i>	8 ← 7	73600.807	0.004	<i>e</i>	8 ← 7	79038.541	0.027
	<i>e</i>	8 ← 7	83138.919	0.008	<i>f</i>	10 ← 9	88203.982	0.003
	<i>e</i>	9 ← 8	83139.341	0.032	<i>f</i>	9 ← 8	88204.406	0.014
	<i>f</i>	8 ← 7	83366.506	0.006	<i>e</i>	10 ← 9	88401.284	-0.007
10 ← 9	<i>f</i>	9 ← 8	83366.936	-0.013	<i>e</i>	9 ← 8	88401.641	-0.013
	<i>e</i>	9 ← 8	92858.025	-0.003				
	<i>e</i>	10 ← 9	92858.378	-0.019				
	<i>f</i>	9 ← 8	93118.952	-0.002				
11 ← 10	<i>f</i>	10 ← 9	93119.392	0.019				
	<i>e</i>	10 ← 9	102562.162	-0.011				
	<i>e</i>	11 ← 10	102562.488	-0.024				
12 ← 11	<i>f</i>	10 ← 9	102857.575	-0.019				
	<i>f</i>	11 ← 10	102857.964	-0.019				
	<i>e</i>	11 ← 10	112251.885	-0.020	<i>f</i>	13 ← 12	116272.310	-0.013
	<i>e</i>	12 ← 11	112252.194	-0.022	<i>f</i>	12 ← 11	116272.661	0.009
13 ← 12	<i>f</i>	11 ← 10	112582.623	0.022				
	<i>f</i>	12 ← 11	112582.992	0.020				
					<i>f</i>		125653.515	-0.011
15 ← 14					<i>e</i>		125992.970	-0.028
	<i>e</i>		141242.289	-0.005	<i>f</i>		144448.893	-0.030
16 ← 15	<i>f</i>		141680.954	0.009	<i>e</i>		144860.942	0.014
					<i>f</i>		153861.682	-0.015
18 ← 17	<i>f</i>		151356.927	0.00	<i>e</i>		154309.767	-0.036
	<i>e</i>		170131.947	-0.045	<i>f</i>		172713.383	-0.026
19 ← 18	<i>f</i>		170678.204	-0.054	<i>e</i>		173232.979	-0.058
	<i>e</i>		179743.519	0.073	<i>f</i>		182150.890	0.071
25 ← 24	<i>f</i>		180325.149	0.033	<i>e</i>		182705.875	0.078
	<i>e</i>		237266.740	-0.031	<i>f</i>		238895.750	-0.025
30 ← 29					<i>e</i>		239656.612	0.018
	<i>e</i>		285066.869	-0.047	<i>f</i>		286286.672	-0.019
38 ← 37	<i>f</i>		286016.697 ^b		<i>e</i>		287211.598	-0.015
	<i>e</i>		361388.690	0.044	<i>f</i>		362204.016	-0.001
	<i>f</i>		362584.458 ^b		<i>e</i>		363380.662	0.000

^aFrequencies calculated with the constants in Table 10.

^bNot included in the fit owing to the perturbation (see Section 3.1.1).

TABLE 7
 MEASURED ROTATIONAL FREQUENCIES IN THE $\alpha^2\Sigma$ EXCITED VIBRATIONAL LEVEL OF C_4H

$N' \leftarrow N$	$J = N - \frac{1}{2}$			$J = N + \frac{1}{2}$		
	$F' \leftarrow F$	Frequency (MHz)	$O - C^a$ (MHz)	$F' \leftarrow F$	Frequency (MHz)	$O - C^a$ (MHz)
2 \leftarrow 1	2 \leftarrow 1	19052.195	0.002	3 \leftarrow 2	19034.551	0.000
				2 \leftarrow 1	19034.559	0.000
3 \leftarrow 2	3 \leftarrow 2	28573.715	-0.003	4 \leftarrow 3	28556.273	-0.002
	2 \leftarrow 1	28574.092	-0.001	3 \leftarrow 2	28556.305	0.002
4 \leftarrow 3	4 \leftarrow 3	38095.249	0.000	5 \leftarrow 4	38077.887	-0.002
	3 \leftarrow 2	38095.401	0.002	4 \leftarrow 3	38077.915	0.002
15 \leftarrow 14		142822.059	0.059		142805.027	0.017
16 \leftarrow 15		152341.151	0.036		152324.186	0.023
18 \leftarrow 17		171378.323	0.027		171361.426	-0.001
25 \leftarrow 24		237995.258	0.061		237978.662	-0.036
30 \leftarrow 29		285563.150	-0.007		285546.928	-0.068
38 \leftarrow 37		361637.717	-0.039		361622.319	0.057

NOTE.—Estimated 1σ uncertainties in the centimeter-wave measurements is 5 kHz.

^aFrequencies calculated with the constants in Table 10.

TABLE 8
 MEASURED ROTATIONAL FREQUENCIES IN THE $b^2\Sigma$ EXCITED VIBRATIONAL LEVEL OF C_4H

$N' \leftarrow N$	$J = N - \frac{1}{2}$			$J = N + \frac{1}{2}$		
	$F' \leftarrow F$	Frequency (MHz)	$O - C^a$ (MHz)	$F' \leftarrow F$	Frequency (MHz)	$O - C^a$ (MHz)
2 \leftarrow 1				3 \leftarrow 2	19000.323	0.005
3 \leftarrow 2	2 \leftarrow 1	28558.709	-0.002	3 \leftarrow 2	28511.978	-0.002
				4 \leftarrow 3	28512.176	0.007
4 \leftarrow 3	3 \leftarrow 2	38070.179	0.012	4 \leftarrow 3	38023.823	-0.004
	4 \leftarrow 3	38070.204	-0.008	5 \leftarrow 4	38023.924	-0.004
8 \leftarrow 7		76114.910	0.035			
9 \leftarrow 8		85625.489	-0.018		85580.757	-0.037
10 \leftarrow 9		95135.697	-0.108		95091.505	-0.118
11 \leftarrow 10		104645.517	-0.168		104602.169	-0.049
12 \leftarrow 11		114154.716	-0.302		114112.540	-0.016
13 \leftarrow 12					123622.556	-0.058
15 \leftarrow 14					142641.738	-0.057
16 \leftarrow 15					152150.770	-0.103
18 \leftarrow 17					171167.819	-0.067
19 \leftarrow 18					180675.774	-0.002
24 \leftarrow 23					228208.117	-0.022
25 \leftarrow 24		237750.637	-0.119		237713.112	0.077
27 \leftarrow 26		256763.157	0.093		256720.966	-0.104
30 \leftarrow 29		285272.924	0.168		285228.362	-0.030
34 \leftarrow 33		323274.033	0.131		323228.432	0.044
35 \leftarrow 34					332726.510	0.011
36 \leftarrow 35		342269.653	0.050		342223.785	-0.024
38 \leftarrow 37		361261.840	-0.090		361215.873	-0.069

NOTE.—Estimated 1σ uncertainties in the centimeter-wave measurements is 5 kHz.

^aFrequencies calculated with the constants in Table 10.

TABLE 9
SPECTROSCOPIC CONSTANTS OF VIBRATIONALLY EXCITED C₄H (PRIOR WORK)

Constant	ground ² Σ ^a	1ν ₇ (² Π) ^b	2ν ₇ (² Σ) ^c	2ν ₇ (² Δ) ^d
<i>A</i>		−89812.6(10)		−50575.69(39)
<i>B</i>	4758.6557(7)	4762.85047(26)	4782.16713(28)	4778.57763(32)
<i>D</i> × 10 ³	0.8627(10)	0.89320(41)	0.91475(57)	0.90125(21)
<i>H</i> × 10 ⁹		0.93(24)	−2.82(38)	
<i>γ</i>	−38.555(2)	−38.149(38)	−56.6483(68)	−37.225(17)
<i>γ_D</i> × 10 ³	0.127(9)	0.030(14)	0.709(26)	
K-type doubling constants:				
<i>p</i>		−18.243(15)		
<i>p_D</i> × 10 ³		0.1809(95)		
<i>q</i>		−14.96761(52)		
<i>q_D</i> × 10 ³		0.11794(36)		
Hyperfine constants:				
<i>a</i>		1.62(49)		1.25(34)
<i>b_F</i> ^e	−14.493	−10.3(15)	−14.62(20)	−20.3(28)
<i>c</i>	12.435(10)	13.6(16)	12.29(21)	11.1(1.9)
<i>d</i>		5.07(72)		
Standard deviation:				
		0.020	0.023	0.020

NOTE.—Units are MHz and uncertainties (in parentheses) are 1σ. The correlation coefficient matrices are available from the authors.

^aFrom Gottlieb et al. (1983).

^bConstants derived from the measurements in Yamamoto et al. (1987) and Table 2.

^cConstants derived from the measurements in Guélin et al. (1987), Yamamoto et al. (1987), and Table 3.

^dConstants derived from the measurements in Yamamoto et al. (1987) and Table 4.

$${}^e b_F = b + \frac{1}{3}c.$$

TABLE 10
SPECTROSCOPIC CONSTANTS OF VIBRATIONALLY EXCITED C₄H (THIS WORK)

Constant ^a	<i>a</i> ² Π	<i>b</i> ² Π	<i>a</i> ² Σ	<i>b</i> ² Σ
<i>A</i>	−7011.1(25)	−152601.3(69)		
<i>B</i>	4778.03697(39)	4770.99746(38)	4760.85127(32)	4755.9431(14)
<i>D</i> × 10 ³	0.80158(87)	0.91582(76)	0.89191(62)	0.9762(17)
<i>H</i> × 10 ⁹	1.04(36)	11.65(33)	2.28(28)	3.94(72)
<i>γ</i>	−34.371(32)	−28.94(19)	−17.266(8)	−46.674(33)
<i>γ_D</i> × 10 ³		1.653(62)	0.409(10)	0.038(18)
<i>K</i> -type doubling constants:				
<i>p</i>	−12.317(21)	−31.716(28)		
<i>p_D</i> × 10 ³		−1.433(48)		
<i>q</i>	2.26473(50)	−16.2750(11)		
<i>q_D</i> × 10 ³	0.04516(36)	0.1889(20)		
<i>q_H</i> × 10 ⁹		−10.42(87)		
Coriolis constants ^a :				
<i>q_I</i>				−0.0728(15)
<i>ρ</i> × 10 ³				−2.5981(99)
Hyperfine constants:				
<i>a</i>		0.0 ^b		
<i>b_F</i> ^c		−7.4(18)	−5.07(13)	−9.27(83)
<i>c</i>		18.9(22)	13.65(25)	6.0(8)
<i>d</i>		3.2(20)		
Standard deviation:				
	0.032	0.034	0.030	0.035

NOTE.—Units are MHz and uncertainties (in parentheses) are 1σ. The correlation coefficient matrices are available from the authors.

^aFor a discussion of the constants see Section 3.1.1, and for the sign conventions see Section 3.1.

^bConstrained to zero.

TABLE 11
 C_4H VIBRATIONAL FREQUENCIES (IN CM^{-1}).

Mode	New levels (This work)	Laser ^a	Theoretical ^b
ν_7		168	178
ν_6	$b^2\Pi$		379
ν_5	$a^2\Pi$		578
ν_4		930	924
ν_3			2131
ν_2			2301
ν_1			3608
$\nu_6 + \nu_7$	$a^2\Sigma$	565	557
$\nu_5 + \nu_7$	$b^2\Sigma$		756

^aFrequencies derived from the electronic spectrum of C_4H using double resonance four-wave mixing (Mazzotti et al. 2011).

^bHarmonic vibrational frequencies at the MCSCF/cc-pVQZ level of theory (Graf et al. 2001).

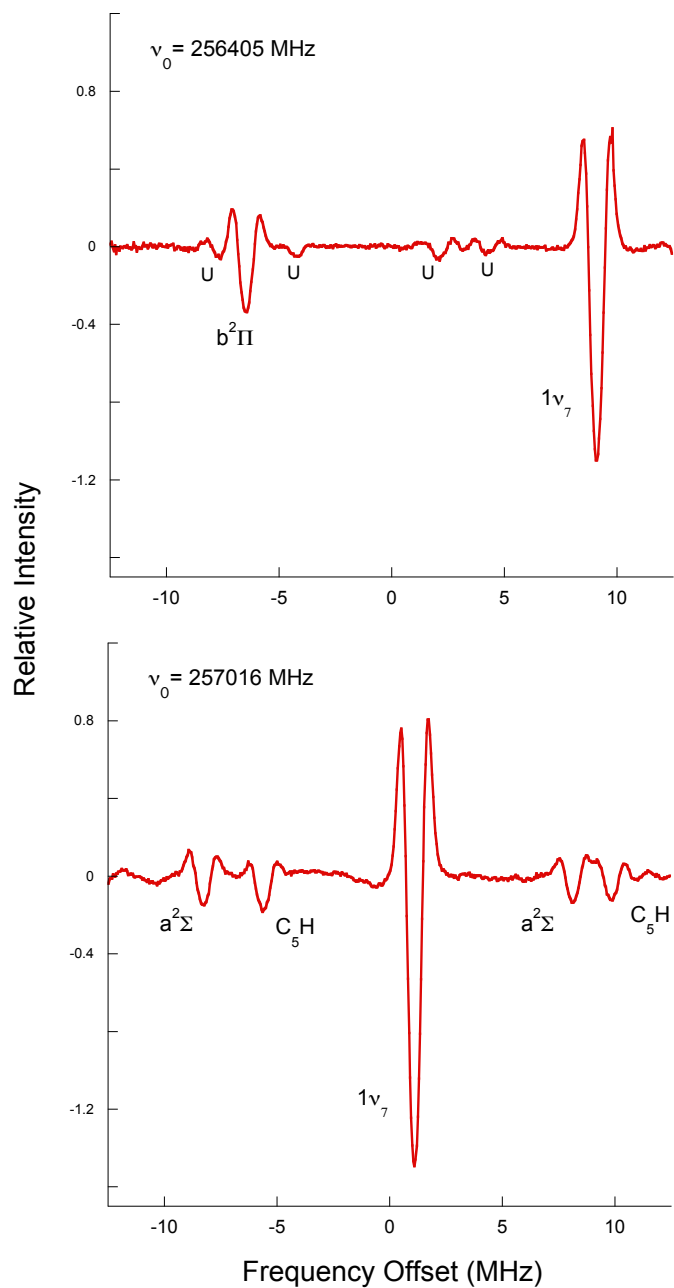


Fig. 1.— Sample rotational spectra of the vibrationally excited C_4H radical. *Upper:* The $J = 26.5 \leftarrow 25.5$ ${}^2\Pi_{1/2}, e$ transition in $b^2\Pi$, and the $J = 26.5 \leftarrow 25.5$ ${}^2\Pi_{1/2}, e$ transition in $1\nu_7$ near 256.4 GHz. The carriers of features labeled U are unidentified. *Lower:* The two spin rotation components of the $N = 27 \leftarrow 26$ transition of $a^2\Sigma$, and the $J = 27.5 \leftarrow 26.5$ ${}^2\Pi_{3/2}, e$ transition in $1\nu_7$ near 257.0 GHz. Also present are the two lambda components of the $J = 53.5 \leftarrow 52.5$ ${}^2\Pi_{3/2}$ transition of the C_5H radical. The line shape is the second derivative of a Lorentzian profile owing to the detection scheme employed. The integration time for each spectrum was approximately 15 min.

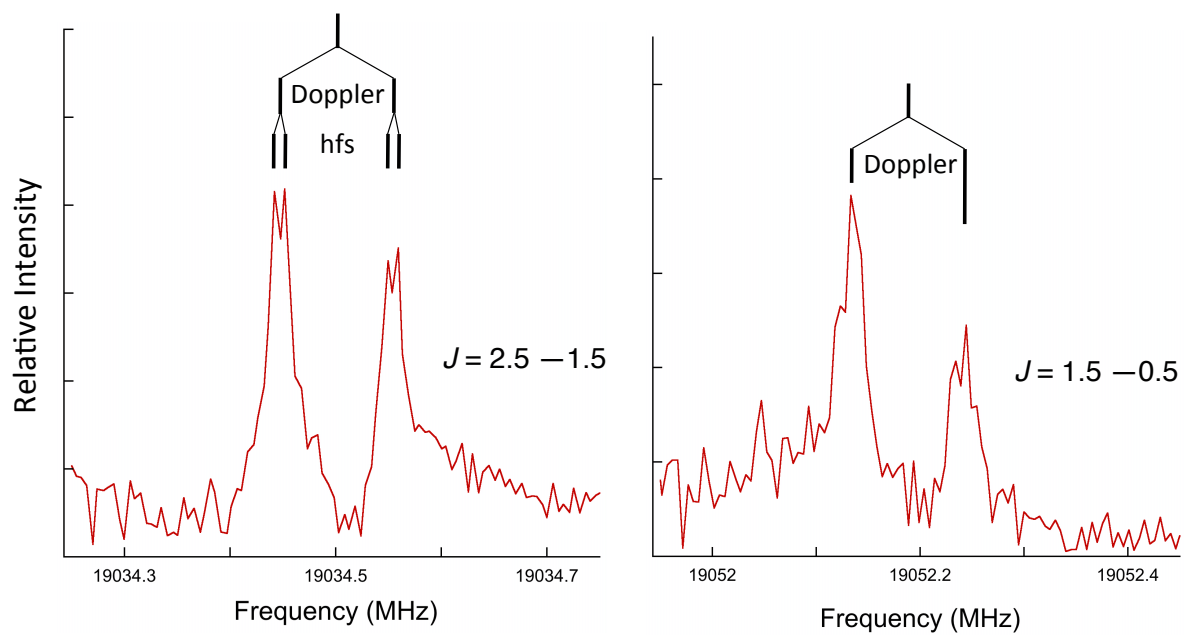


Fig. 2.— Sample rotational spectra in the two spin rotation components of the $N = 2 \rightarrow 1$ rotational transition in the $a^2\Sigma$ excited vibrational level of C_4H observed in a supersonic molecular beam. Partially resolved hyperfine structure is observed in the $J = 2.5 - 1.5$ component. The integration time was 12 min at 19034 MHz and 20 min at 19052 MHz.

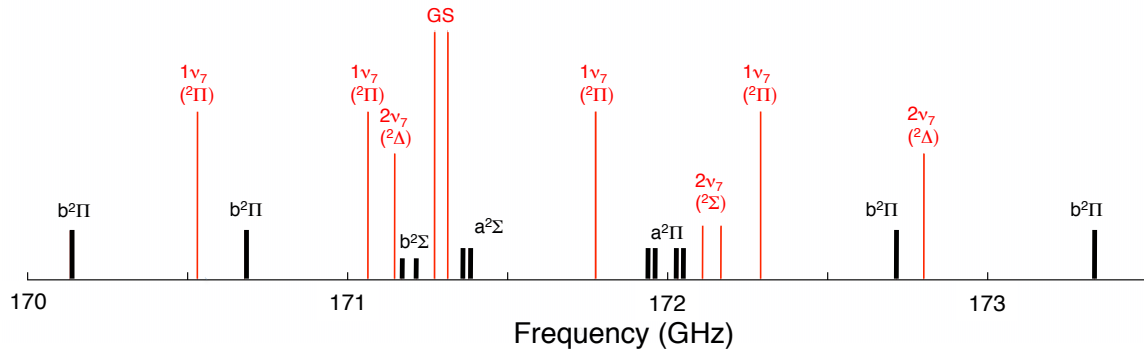


Fig. 3.— Stick spectrum of the $N = 18 \leftarrow 17$ rotational transition in the ground and excited vibrational levels of C_4H near 171 GHz. *Red*: Three vibrationally excited levels identified previously by Yamamoto et al. (1987), and the $^2\Sigma$ electronic ground state ground state (GS). *Black*: The four new vibrational levels $a^2\Pi$, $b^2\Pi$, $a^2\Sigma$, and $b^2\Sigma$ (this work). The relative intensities were measured in a low pressure discharge through helium and acetylene (see Section 2.1).

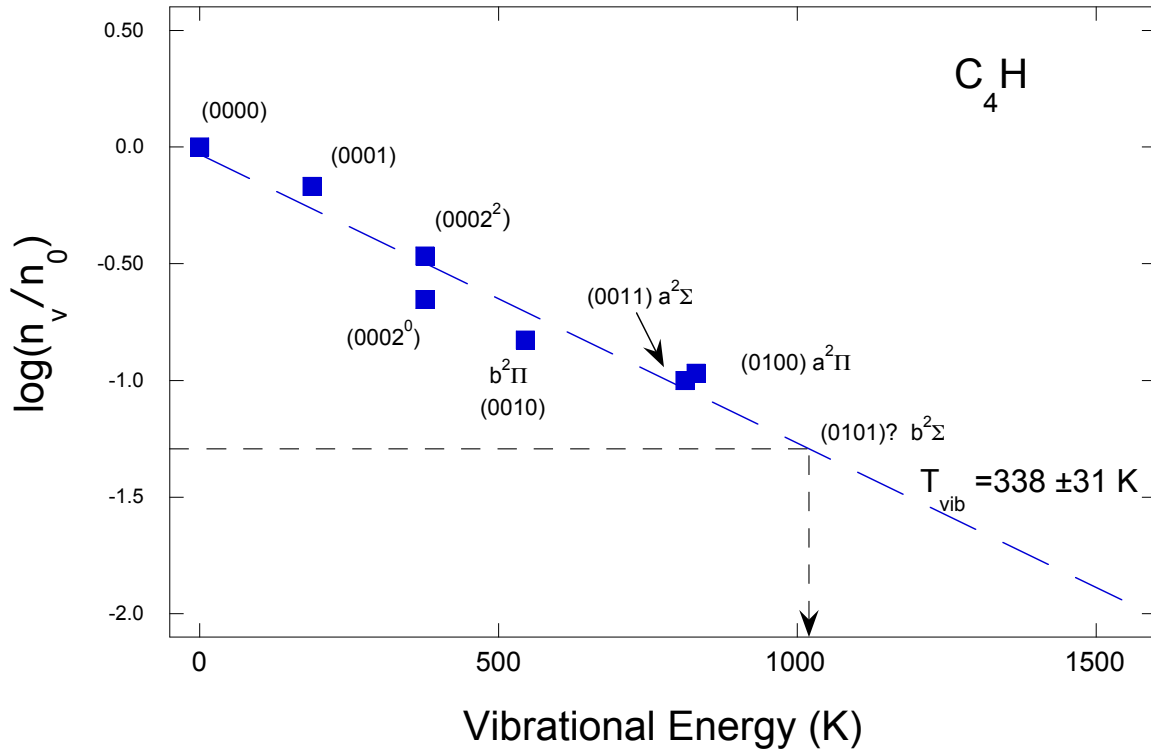


Fig. 4.— Vibrational temperature diagram of the $1\nu_7$, $2\nu_7$, and four new levels of C_4H in the $X^2\Sigma$ electronic state. The relative populations in the ground (n_0) and excited vibrational levels (n_v) were determined from measurements of the $N = 15 \leftarrow 14$ rotational transition near 143 GHz in a low pressure discharge through He and HCCH cooled to 150 K. The vibrational levels are labeled as $(\nu_4, \nu_5, \nu_6, \nu_7)$. See Sections 3.1.3 and 3.1.4 for a discussion of the assignments of the new levels.

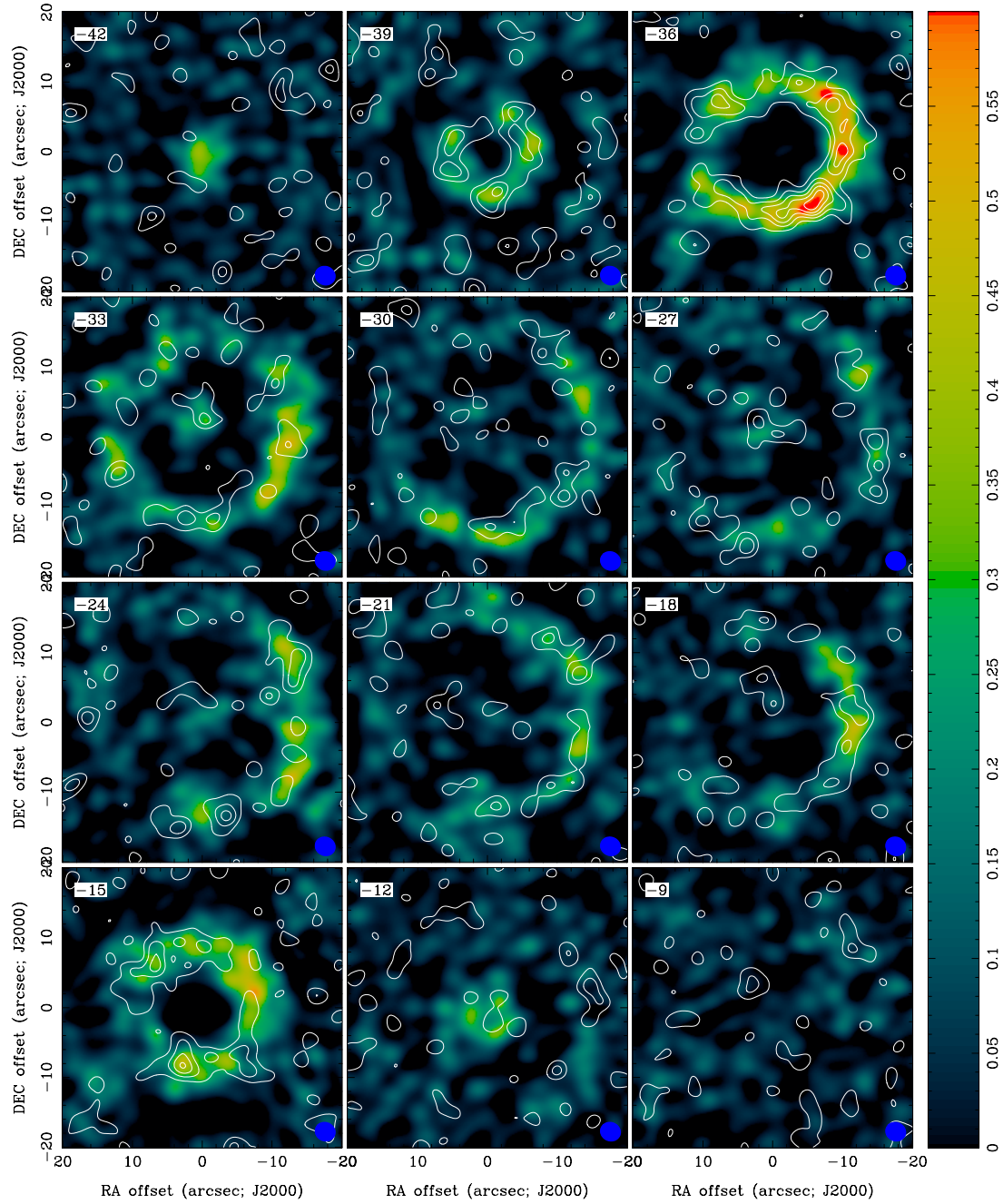


Fig. 5.— Velocity channel maps of the $N = 27 \rightarrow 26$ rotational transition of C_4H in the ground and $1\nu_7$ ($^2\Pi$) excited vibrational level. *Color half-tone*: average of the two spin doublets in the ground vibrational state at 256880 and 256919 MHz at $E_u = 173$ K. *White contours*: average of three of the four lambda components of the $1\nu_7$ ($^2\Pi$) level at 256414, 257017, and 257218 MHz at $E_u = 363$ K. The contours are plotted every 3σ , starting with 3σ and an rms noise of 20 mJy/beam. The actual rms noise varies in each channel map, but is approximately 20 to 50 mJy/beam. The maps show the close correspondence between the ground and excited state emission, and the azimuthal asymmetry and clumpiness in the expanding outer shell.

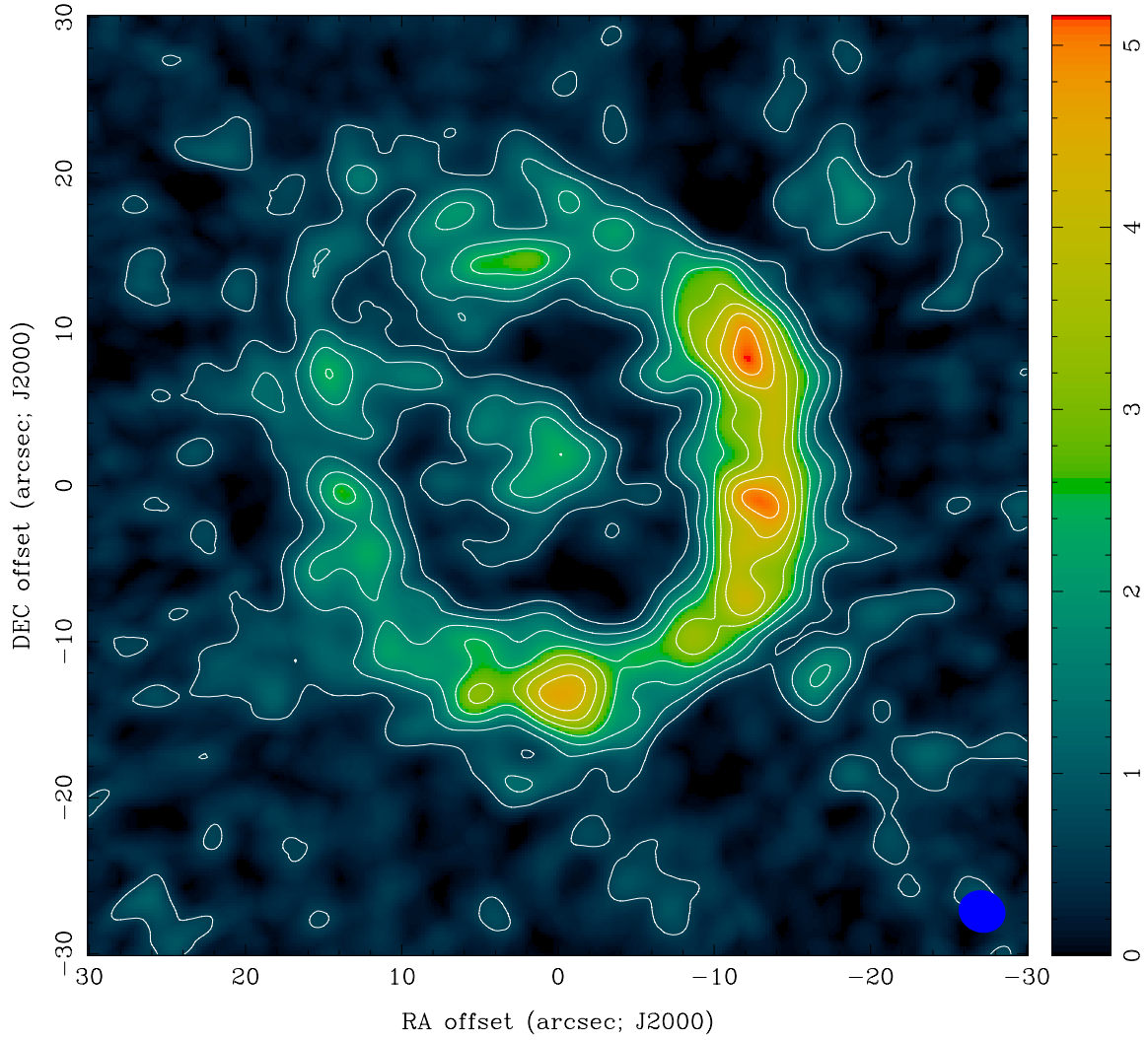


Fig. 6.— Integrated intensity map of the ground state emission of C₄H (see Figure 5). The velocity range of integration (-33 to -18 km s⁻¹) is approximately centered on the systemic velocity. The emission near the center shows that C₄H is not confined solely to the outer envelope.

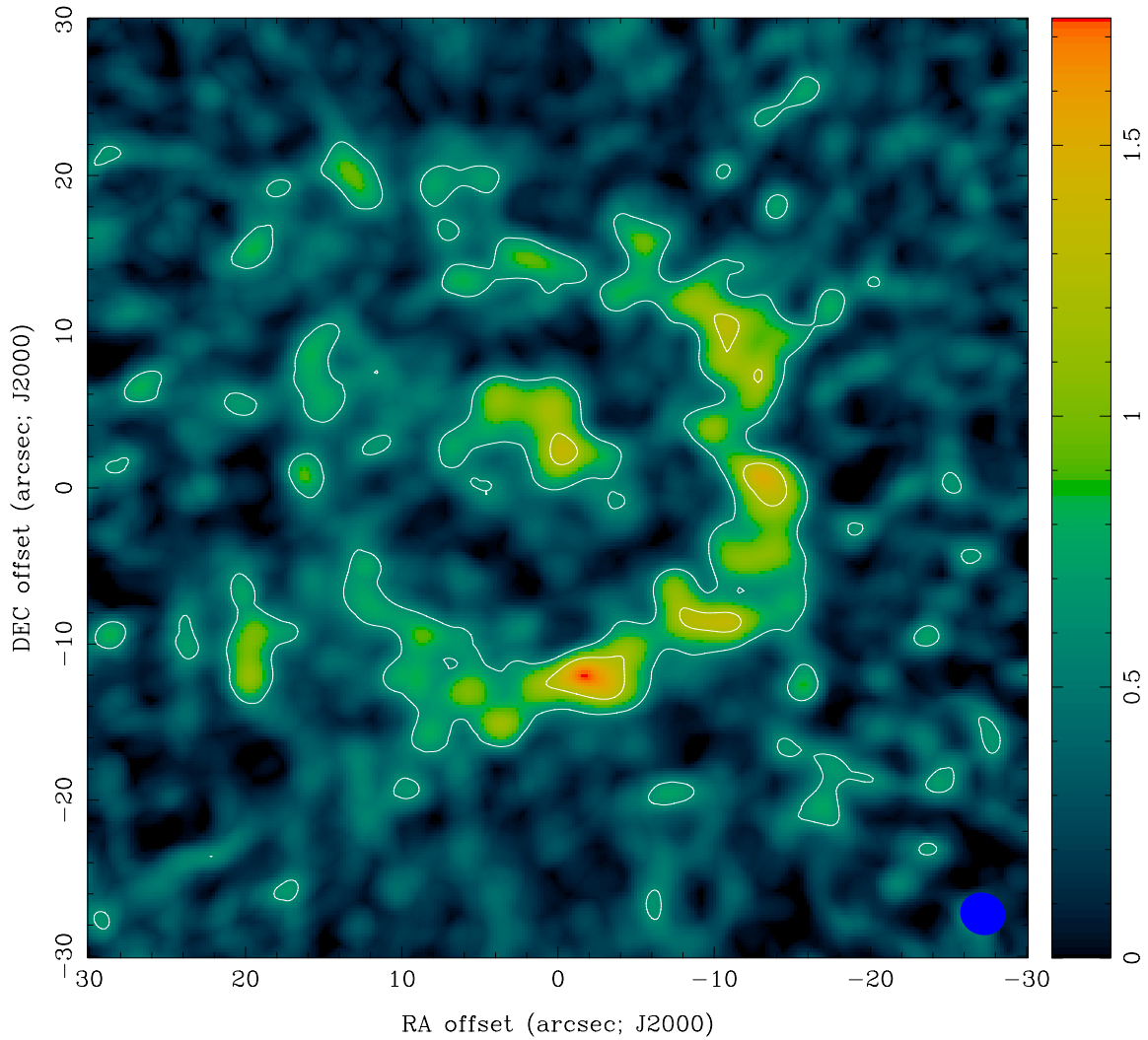


Fig. 7.— Integrated intensity map of C₄H of the $1\nu_7$ excited vibrational level (see Figure 5). The velocity range of integration (-33 to -18 km s⁻¹) is approximately centered on the systemic velocity. The map here of the integrated intensity of the $1\nu_7$ level confirms that C₄H is present close to the star. The clumps seen in the outer ring correlate well with those seen in the ground state emission in Figure 6.